

COVER PAGE

Document downloaded by @DAEL

Fri Nov 27 10:23:48 2026
For personal use

When automatic English translation is provided, only the original document is authentic.
The EAA cannot be held responsible of any translation error

Bibliographical reference

Experiments on Active Control of Counter-Rotating Open Rotor Interior Noise, T. Haase, S. Algermissen, O. Unruh and M. Misol, Acta Acustica **vol. 100** (Number 3), 2014, pp. 448-457

DOI
https://doi.org/10.3813/AAA.918725

Acta Acustica united with Acustica
Vol. 100 (2014) 448 – 457

DOI 10.3813/AAA.918725

Experiments on Active Control of Counter-Rotating Open Rotor Interior Noise

T. Haase, S. Algermissen, O. Unruh, M. Misol
Department of Adaptive Systems, German Aerospace Center (DLR), Lilienthalplatz 7, 38108 Braunschweig, Germany. thomas.haase@dlr.de

Summary
The efficiency of future aircraft has to be increased because of the CO_2 restrictions layed down by the European Union. Two key technologies to reach this ambitious goal are a consequent lightweight design of future aircraft and new engine concepts like the Counter-Rotating open rotors (CROR). However, the combination of lightweight materials like carbon-fibre-reinforced plastics (CFRP) with CROR is acoustically demanding because of the very high sound pressures emitted by this type of engine and the poor transmission loss of CFRP structures in the lower frequency range. Therefore, this work conducts a preliminary study to improve the transmission loss of a CFRP panel excited by a synthesised CROR pressure field in lower frequency range. As a first step, a typical aircraft fuselage panel mounted in a sound transmission loss facility is equipped with actuators and sensors to implement multiple-input multiple-output (MIMO) feedforward control of flexural vibration. The CFRP panel is excited via a CROR pressure field synthesised by a 112-channel loud speaker array. The active vibration control (AVC) system is realised by accelerometers and inertial exciters. A considerable vibration reduction of the flexural vibration on the accelerometers is achieved. The local attenuation around the accelerometers leads to a new controlled vibration pattern that radiates sound in a different way than the uncontrolled one. The difficulties in reducing the radiated sound power through the AVC system are due to low observability, the "pinning" effect, and the restructured vibration patterns. All of these effects are studied in detail through surface vibration scans and sound intensity measurements. Additionally, the radiation resistance matrix is used to analyse the controlled vibration patterns.

PACS no. 43.40.Dx, 43.40.-r, 43.40.+s

1. Introduction

Due to the future CO_2 regulation of the European Union, the commercial aviation industry has been forced to investigate new engine concepts and new lightweight designs. A possible solution to fullfill these regulations is a consequent lightweight design with carbon-fibre-reinforced plastics (CFRP) and the use of counter-rotating open rotor (CROR) engines. The combination of these technologies is acoustically challenging because of the poor transmission loss of CFRP and the high sound pressure levels emitted by the CROR in the lower frequency range [1, 2].

Active concepts offer a lightweight-compliant solution for the improvement of transmission loss in the lower frequency range, while the very high mass requirements of passive damping systems render them impractical in this frequency range. So during the last 20 years, many active concepts for the solution of sound radiation problems have been investigated, see for example the review papers [3] and [4].

Received 27 September 2013,
accepted 21 February 2014.

Active noise control (ANC) is a widely known approach for the reduction of noise levels. A lot of theoretical and experimental work on ANC has focused on cavities [5] and double wall cavities [6]. A very complex load master area of the A400M was controlled by an ANC system [7], while Cabell *et al.* [8] conducted an experimental flight test of an ANC system.

Another approach is the active structural acoustic control (ASAC), which is mainly used for the reduction of sound radiation of plates [9, 10] and more complex structures like car windshields [11] and truck oil pans [12]. Preliminary studies by Fuller *et al.* [13] show a significant sound reduction of 11 dB on two control microphones in a very small-scale fuselage model. A complex flight test of an active system was conducted by Palumbo *et al.* [14] in which 21 actuators were placed on the aircraft fuselage and 32 microphones placed inside the cabin to control the interior noise. A reduction of 10 dB for the blade passing frequencies could be obtained. Nevertheless, these investigations typically use microphone error sensors, which can lead to an increased vibration of the fuselage that acts like a loudspeaker in such a system. Furthermore, Gardonio in his review article [15] describes the problem of fatigue caused by mounting and driving the secondary actuators

© S. Hirzel Verlag · EAA

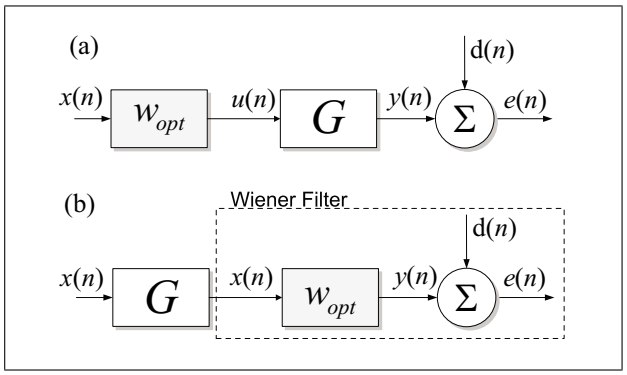

Figure 1. Block diagram of a feedforward control system for physical implementation (a) and for filter calculation (b).

on the primary aircraft skin. It is already known that the ASAC approach is superior to AVC in reducing sound radiation. Yet ASAC systems need a lot of sensors in order to estimate the sound power through the use of the radiation modes method and can also increase the flexural vibrations of the fuselage. In comparison to ASAC, AVC systems can reduce the vibration and the interior noise simultaneously.

To give an example, Grewal *et al.* [16] used AVC to reduce the vibration of a fuselage skin and simultaneously reduce the interior noise of a deHavilland Dash-8. In this study, a pure tone at the blade passing frequency is reduced by 28 dB in interior noise and by 16 dB in the vibration of the fuselage.

To the author′s best knowledge, only a little work has been done to further study AVC systems' adequacy for reducing vibration and interior noise on detailed aircraft structures under real excitation.

Therefore, this study shall demonstrate the possibility of using an active feedforward vibration control system with structural actuators and sensors to improve the low frequency transmission loss of a CFRP fuselage panel excited by a synthetic multisinusoidal CROR sound pressure field. The paper presents the experiments carried out on an aircraft-relevant fuselage panel in a sound transmission loss test facility. Furthermore, the performance of the control system regarding the local/global vibration reduction and the sound radiation are studied in detail.

The paper is subdivided as follows: In section 2, the theoretical background of the causal controller used in the experiments and the derivation of the radiation resistance matrix is described. A description of the CFRP fuselage structure and the active feedforward vibration control systems used in this study is given in section 3. Section 4 provides a brief introduction into the sound field synthesis used to generate the multisinusoidal pressure field. The system identification used for the offline calculation of the controller is presented in section 5.1. A detailed discussion of the active vibration control system and its effects on the sound radiation of the fuselage skin are shown in section 5.2. The radiated sound power is analysed by means of surface vibration scans, the radiation resistance matrix and measurements with a sound intensity probe. The conclusions are given in section 6.

2. Theory

In the experiments described in section 3 a multiple-input multiple-output (MIMO) feedforward vibration controller is used. In order to describe the experimental offline calculation of the feedforward controller a short introduction for the single-input single-output (SISO) case is given in section 2.1. Because of the known difficulties in the reduction of the sound radiation with an active vibration control system, the controlled structure will be analysed by surface vibration scans and the radiation resistance matrix. A brief introduction to the derivation of the radiation resistance matrix is given in section 2.2.

2.1. Causal feedforward control

Multisinusoidal excitations are the best application scenario for an active adaptive feedforward control system, because a coherent reference signal can easily generated from the rotation frequencies of the CROR engine. Furthermore, this kind of reference signal is not disturbed by any feedback effects of the active feedforward controller, which influences the stability of the active control system [17]. Its stability (90Âř phase margin) and its robustness (adaptive algorithm) make a CROR excitation the typical scenario for an adaptive feedforward controller the latter of which can be further improved by online secondary path modeling techniques. Yet in order to be able to evaluate the performance of an adaptive feedforward control system in steady state without having to wait until convergence, an optimal feedforward controller is implemented. This optimal feedforward controller exactly predicts the performance of an adaptive feedforward controller for stationary excitations [18]. To give a short summary of how the optimal filter is derived in the experiments a brief description of a SISO optimal causal feedforward controller is given here; for detailed information about the MIMO version see [18].

A typical block diagram of a feedforward controller is presented in Figure 1. If we assume that the optimal filter $\mathbf{w_{opt}}$ and the secondary path transfer function $\mathbf{G}$ are linear time-invariant systems, the order of the systems can be reversed [18]. Reversing $\mathbf{G}$ and $\mathbf{w_{opt}}$ allows the application of the classical Wiener Filter theory by using filtered reference signals $x'(n)$. These filtered refer ence signals can be evaluated for the SI SO case by

$$x'(n) = \sum_{r=0}^{R-1} g_r x(n-r), \tag{1}$$

in which $x(n)$ is the reference signal at the discrete time n, g_r are the coefficients of a finite impulse response (FIR) filter representing the secondary path, and R is the length of the secondary path FIR filter. A quadratic cost function of the error signals is assumed

$$J = E\left[e(n)^T e(n)\right] \tag{2}$$

in which $E[\cdot]$ is the expectation operator. Assuming that the signals are stationary and ergodic, the expectation operator can be calculated by averaging over time. Referring

to Figure 1b, the Wiener Filter can be calculated by using the autocorrelation matrix $\mathbf{R}_{\mathbf{x'x'}}$ of the filtered reference signal, the crosscorrelation vector $\mathbf{r}_{\mathbf{x'd}}$ of the filtered reference signal, and the disturbance signal $d(n)$ [18].

$$\mathbf{w_{opt}} = {\mathbf{R}_{\mathbf{x'x'}}}^{-1}\mathbf{r}_{\mathbf{x'd}}. \tag{3}$$

Now, writing the filtered reference signal as a vector of length L

$$\mathbf{x'}(n) = \left[x'(n)x'(n-1)\cdots x'(n-L+1)\right], \tag{4}$$

the auto- and crosscorrelation matrix of the filtered reference signal can be described by

$$\begin{aligned}\mathbf{R}_{\mathbf{x'x'}} &= E\left[\mathbf{x'^T}(n)\mathbf{x'}(n)\right] \\ &= \begin{pmatrix} r_{x'x'}(0) & r_{x'x'}(1) & \dots & r_{x'x'}(L-1) \\ r_{x'x'}(1) & r_{x'x'}(0) & \dots & r_{x'x'}(L-2) \\ \vdots & \dots & \ddots & \vdots \\ r_{x'x'}(L-1) & r_{x'x'}(L-2) & \dots & r_{x'x'}(0) \end{pmatrix}\end{aligned} \tag{5}$$

with

$$r_{x'x'}(k) = E\left[x'(n)x'(n-k)\right]. \tag{6}$$

The autocorrelation matrix is symmetric and therefore it is assumed that

$$r_{x'x'}(k) = r_{x'x'}(-k). \tag{7}$$

The crosscorrelation vector is described by

$$\begin{aligned}\mathbf{r}_{\mathbf{x'd}} &= E\left[\mathbf{x'^T}(n)d(n)\right] \\ &= \left[r_{x'd}(0) \quad r_{x'd}(1) \quad \dots \quad r_{x'd}(L-1)\right]^T.\end{aligned} \tag{8}$$

The performance of the systems can be evaluated in terms of the residual error signal

$$e(n) = d(n) - \sum_{r=0}^{R-1} g_r \mathbf{w_{opt}^T}\mathbf{x}(n-r), \tag{9}$$

in which $\mathbf{x}(n)$ is the reference signal vector of length L described by

$$\mathbf{x}(n) = \left[x(n) \quad x(n-1) \quad \dots \quad x(n-L+1)\right]^T. \tag{10}$$

The calculation of the optimal feedforward controller for the experiments is conducted as follows:

- Identification of the secondary path
- Synchronous measurement of the reference signal and the disturbance signal
- Offline calculation of the optimal filter with equation (3)
- Implementation of the filter taps into the Digital Signal Processor (DSP)

2.2. Radiation resistance matrix and radiation efficiency

In order to study the radiated sound power of the fuselage panel caused by the vibration pattern of the control area, the radiation resistance matrix (RRM) is used. Through the RRM, the radiated sound power of the control area can be calculated via the measured surface velocities. To derive the RRM, the elemental radiator approach is used, see [19].

By choosing a discretisation of the vibrating area that renders the elemental rectangular radiators small compared to the structural and acoustic wavelengths, the radiated sound power can be described by [19]

$$P(\omega) = \frac{S}{2N} Re\left\{{\mathbf{v_e}}^H(\omega)\cdot\mathbf{p_e}(\omega)\right\}, \tag{11}$$

where $\mathbf{v_e}$ and $\mathbf{p_e}$ are the complex column vectors of the surface velocities and pressures of each elemental radiator, N is the number of elemental radiators, the superposed S is the area of the entire vibrating surface, and ^{H} means the hermitian transpose. The pressures in front of each element can be calculated with the velocities of all elemental radiators with the impedance matrix $\mathbf{Z}$

$$\mathbf{p_e}(\omega) = \mathbf{Z}(\omega)\cdot\mathbf{v_e}(\omega). \tag{12}$$

The sound power can then be calculated by

$$P(\omega) = \frac{S}{2N} Re\left\{{\mathbf{v_e}}^H(\omega)\cdot\mathbf{Z}(\omega)\cdot\mathbf{v_e}(\omega)\right\}. \tag{13}$$

According to [19], the RRM is described by

$$\begin{aligned}\mathbf{R}(\omega) &= \frac{S}{2N} Re\left\{\mathbf{Z}\right\} \\ &= \frac{\omega^2\rho_0 S_E^2}{4\pi c_0}\begin{bmatrix} 1 & \frac{sin(kr_{12})}{kr_{12}} & \dots & \frac{sin(kr_{1N})}{kr_{1N}} \\ \frac{sin(kr_{21})}{kr_{21}} & 1 & & \vdots \\ \vdots & & \ddots & \vdots \\ \frac{sin(kr_{N1})}{kr_{N1}} & \dots & \dots & 1 \end{bmatrix},\end{aligned} \tag{14}$$

where ρ_0 is the density of air, S_E is the area of an elemental radiator, k is the wave number, c_0 is the speed of sound in air, and r_{xy} is the distance of elemental radiator x to elemental radiator y. The radiated sound power can now be described by the RRM and the normal surface velocities:

$$P(\omega) = {\mathbf{v_e}}^H(\omega)\cdot\mathbf{R}(\omega)\cdot\mathbf{v_e}(\omega) \tag{15}$$

Further information about the sound radiation can be gathered by using the radiation efficiency, which describes the ability of a vibration pattern to radiate sound in reference to a uniformly vibrating piston [19]. The radiation efficiency σ is given by

$$\sigma(\omega) = \frac{P(\omega)}{\rho_0 c_0 S\left\langle\bar{v_n^2}(\omega)\right\rangle}, \tag{16}$$

where $\langle\bar{v_n^2}\rangle$ is the normal averaged quadratic surface velocity.

Table I. Properties of the fuselage.

Property	Unit
Material	CFRP quasi-isotropic
Layers	8
Thickness per layer	0.25 mm
Radius	2,820 mm
Stiffeners	Vertikal: T-Shape 5 mm Horizontal: L-Shape 2 mm

Table II. Hardware for experiments.

Device	Type	Add. data
Accelerometer	PCB 352A24	m = 0.8 [g]
Exciter	Visaton EX45	m = 60 [g] P = 10 [W]
Low-pass filter	Kemo Card Master 255G	F_c = 960 [Hz] 24 [dB/Oct.]
Real-time system	dSpace DS1006	F_s = 2000 [Hz]
Sound intensity probe	Bruel & Kjaer	Type 3599
Laser scanning vibrometer	Polytec PSV 400	-

3. Experimental setup

In this section, the experimental setup is described. A CFRP fuselage with aluminium stiffeners is mounted in the test opening of the transmission loss test facility of the German Aerospace Center (DLR). The geometrical properties of the fuselage are presented in Table I.

The fuselage panel is mounted on four shock mounts, which are connected to the top and bottom of the outer vertical stiffeners. A picture of the fuselage panel is shown in Figure 2 (view from anechoic room). The fuselage panel is excited by a 112-channel speaker system, where each of the 112 channels can be controlled individually to synthesise sound pressure fields.

The array is used to generate a multisinusoidal CROR pressure field, which is predicted by a simulation conducted at the DLR [20].

The control systems used in this study are MIMO feedforward control systems. One of the 112 speaker driving signals is used as reference signal for the feedforward controller. This is an acceptable assumption for the practical implementation because the reference signal could be gathered from the CROR engines in a possible technical realisation. Furthermore, 10 inertial exciters are used as secondary actuators. This type of actuator applies a dynamic force on its host structure through a the moving mass excited by a magnetic field. The error signals determining the MIMO version of the quadratic cost function presented in equation (2) are measured by 10 or 17 accelerometers. The feedforward control system is visualised in Figure 4.

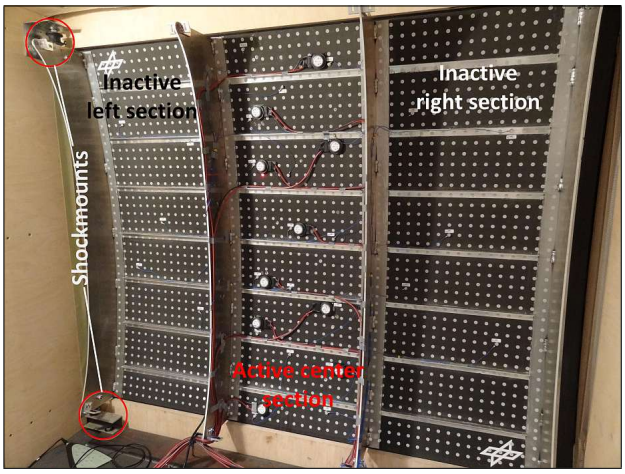

Figure 2. CFRP fuselage with stiffeners in the sound transmission loss facility.

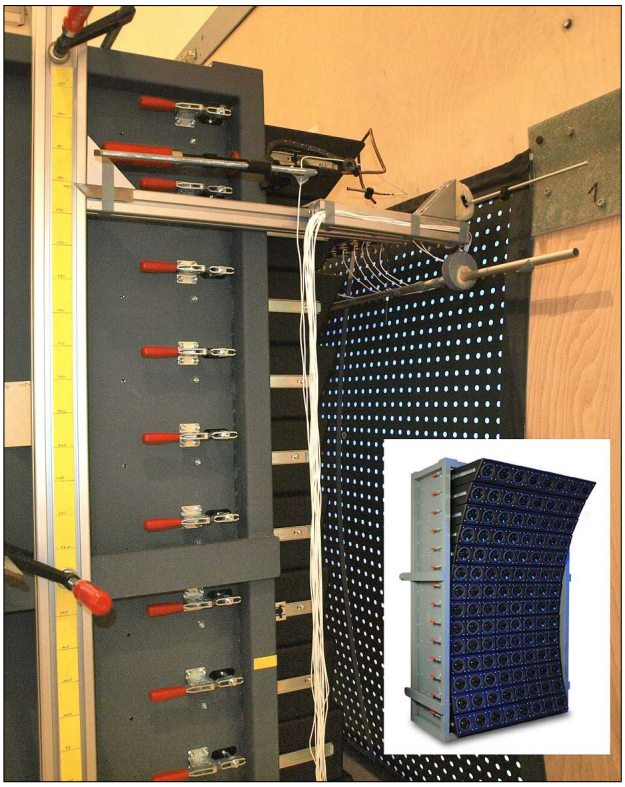

Figure 3. Speaker array in the reverberation room.

In summary, two feedforward active vibration control systems are investigated. First, a nearly collocated control system consisting of the speaker reference, 10 inertial secondary exciters and 10 nearly collocated accelerometers used as error sensors is studied. Deviating from the usual definition of a collocated sensor/actuator pair, closely collocated in this study means that the sensor is placed geometrically as close as possible to the actuator. The reason for studying this kind of configuration is its improved vibration control performance, which is discussed in [21]. The second system consists of the equipment of the nearly collocated system and seven additional accelerometers

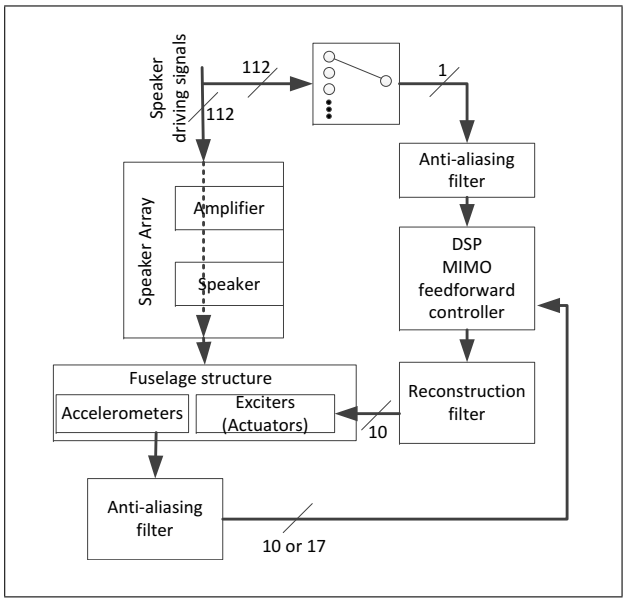

Figure 4. Flowchart of the experimental control system.

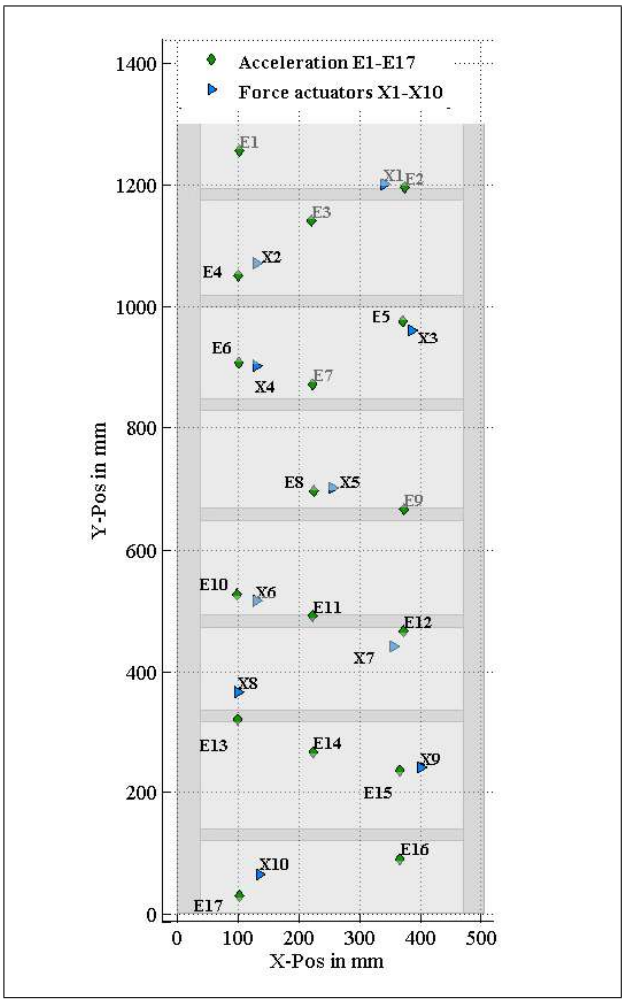

Figure 5. Actuator and sensor positions on the centre section of the fuselage.

used as error sensors. The advantage of this system lies in the higher observability due to the 17 error sensors.

The placement of the actuators and sensors is shown in Figure 5. It has to be mentioned that the actuator placement is a preliminary placement in that the actuators are distributed empirically over the control surface. A list of the hardware equipment used in this experiment is presented in Table II.

It is important to note that only the fuselage panels centre section has been equipped with sensors and actuators (see Figure 2). The analysis of the vibration and sound radiation is thus focused on this active section.

In addition to the local vibration attenuation, achieved by the control systems by means of the accelerometers, surface vibration scans and sound intensity measurements are made. These measurements are used to analyse the sound radiation of the structure under the influence of the feedforward vibration control systems.

4. Sound field synthesis

In order to present an overview of the sound field synthesis, a short summary of the CROR sound field synthesis is presented in the following; further details can be found in [20]. More informations about the sound field synthesis for different excitations can be found in [22] and [23].

For the synthesis of the desired CROR pressure field, the frequency response functions (FRF) of the 112-channel speaker array to 110 microphone positions are measured. In an experiment, these numerous transfer paths cannot be measured simultaneously. Therefore, sequential measurements with a travelling 10 microphone line array and a reference microphone are conducted. Experiments with a MIMO identification system lead to poor identification results, therefore a single-input multiple-output identification scheme is used [20]. One excitation speaker and 10 microphones plus a reference microphone are measured simultaneously.

For the derivation of the speaker driving signals, a matrix inversion problem has to be solved. Assuming a linear transfer matrix from speakers to microphones, the pressure $\mathbf{p}(j\omega)$ can be described by

$$\mathbf{p}(\mathrm{j}\omega) = \mathbf{G_{pu}}(\mathrm{j}\omega)\mathbf{u}(\mathrm{j}\omega), \tag{17}$$

where $\mathbf{G_{pu}}(\mathrm{j}\omega)$ is the transfer matrix at frequency ω and $\mathbf{u}(\mathrm{j}\omega)$ is the driving signal matrix of the loudspeakers. The transfer matrix $\mathbf{G_{pu}}(j\omega)$ describes the path from the loudspeaker driving signals to the microphones (including the amplifier, loudspeaker, fluid, and microphone dynamics). By using the pseudo inverse of the transfer matrix, which always exist if the number of loudspeakers is greater than or equal to the number of microphones, we can derive the desired loudspeaker signals. Assuming $\mathbf{p}^*(\mathrm{j}\omega)$ are the desired pressure values, then

$$\mathbf{u}(\mathrm{j}\omega) = \mathbf{G_{pu}}^{+}(\mathrm{j}\omega)\mathbf{p}^*(\mathrm{j}\omega), \tag{18}$$

where the pseudo inverse $\mathbf{G_{pu}}^{+}(\mathrm{j}\omega)$ is given by

$$\mathbf{G_{pu}}^{+}(\mathrm{j}\omega) = \mathbf{G}_{pu}^{H}(\mathrm{j}\omega)\left(\mathbf{G}_{pu}(\mathrm{j}\omega)\mathbf{G}_{pu}^{H}(\mathrm{j}\omega)\right)^{-1}, \tag{19}$$

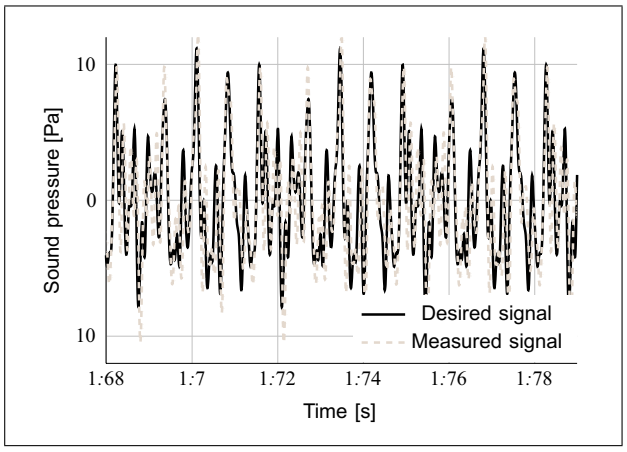

Figure 6. Reproduction quality in time domain.

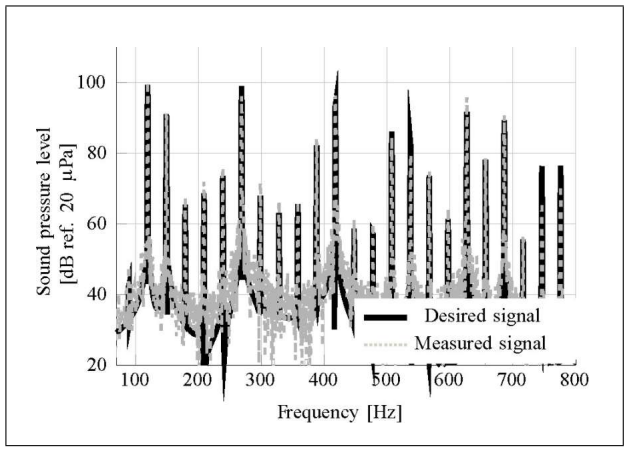

Figure 7. Reproduction quality in frequency domain.

where the superposed ^{H} means the hermitian transpose. An example of the sound reproduction quality in time domain, which is measured in the transmission loss facility at one of the microphones, is given in Figure 6. An averaged sound pressure spectrum over all microphones is given in Figure 7 for a 56-loudspeaker 30-microphone system.

5. Feedforward control results

In this section, the results of the feedforward control system are presented. First of all, the system identification is described. Afterwards, the experimental control results of the preliminary study in the sound transmission loss facility are presented.

5.1. System identification

Referring to equation (1), a precise secondary path model **G** is needed to calculate the filtered reference signals. A multi-reference test is conducted to derive a state space model of the secondary path. Therefore, the actuators are driven by band-limited uncorrelated white noise signals and the sensor signals are sampled simultaneously. The oversampling method is used to enhance the signal-to-noise ratio (SNR) of the identification process. By downsampling the measured time data to the desired sampling frequency of 2,000 Hz and through post-processing by a subspace-based identification algorithm [24], an accurate state space model of the secondary path is derived. The model quality can be seen in the singular values of the identified state space model and the estimated FRF's depicted in Figure 8. Due to the actuator and sensor characteristics, the SNR is insufficient for the identification of a precise model in the frequency range from 0 Hz to 100 Hz. Nevertheless, there is a very good alignment in the range of the CROR frequencies from 110 Hz up to 700 Hz. The identified model of the fuselage panel has 900 states. A smaller number of states did not lead to sufficient identification results.

5.2. Feedforward control of the fuselage panel

After the reproduction of the sound field, the uncontrolled vibration patterns of the fuselage in the sound transmission

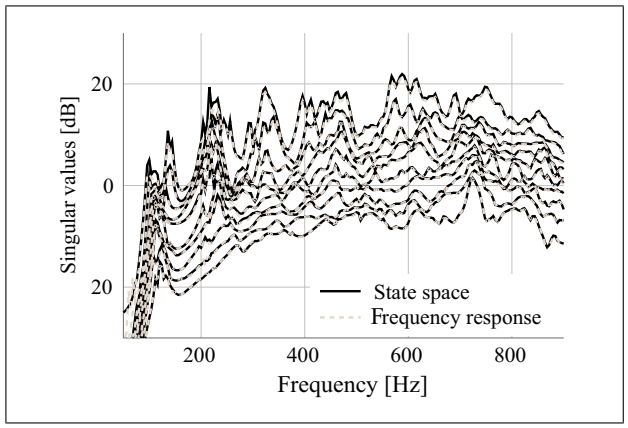

Figure 8. Singular values of the fuselage model.

loss facility are measured with a laser scanning Doppler vibrometer (LSV). Three examples of the centre section of the CFRP fuselage without control are presented on the left side of Figures 12, 13, and 14. To the authors' surprise, the first two CROR frequencies excite the panel mainly at the edges of the outer inactive sections. This is due to the boundary conditions of the fuselage panel, which is mounted only at the corners of the outer stiffeners so that the edges of the fuselage panel are free. Therefore, no improvements for these two frequencies can be achieved by using a control system in the centre section and so they are neglected in this study.

To implement the optimal feedforward controller, the FIR filter taps are derived with equation (3). The taps are implemented in the Simulink® control scheme and, afterwards, the local vibration attenuation at the error sensors, the global vibration attenuation with the LSV, and the radiated sound power are measured with the controller switched on and off. Since the sound power has been measured only inside the two stiffeners, it is disturbed by their vibration and by the vibration of the passive outer sections of the CFRP fuselage panel. To calculate a dedicated sound power reduction of the vibrating control area, the measured surface velocities are post-processed with the RRM in order to derive the radiated sound power.

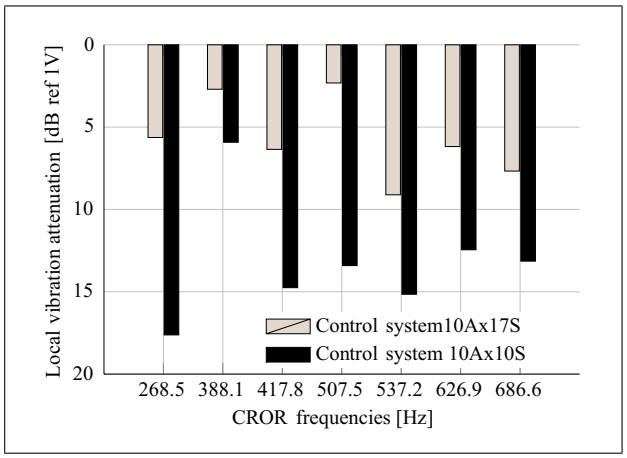

Figure 9. Local vibration attenuation of the fuselage panel.

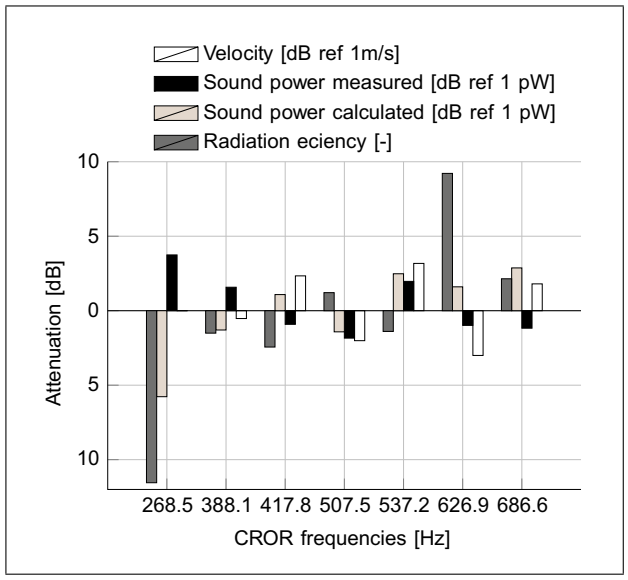

Figure 10. Attenuations between Control On and Off for the 10-sensor 10-actuator system.

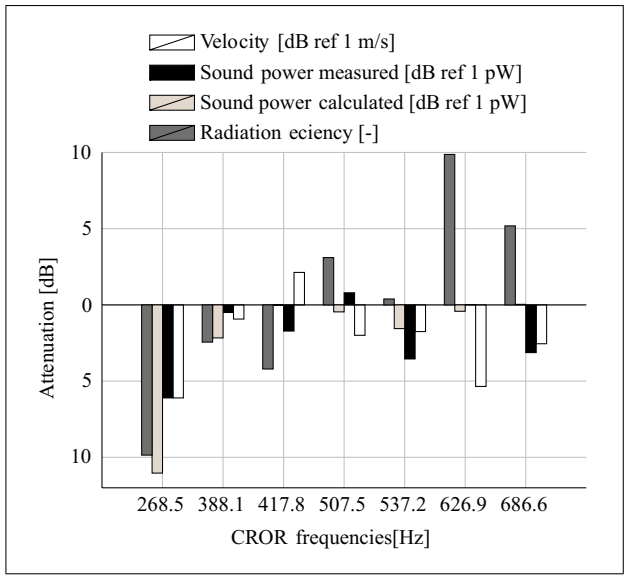

Figure 11. Attenuations between Control On and Off for the 17-sensor 10-actuator system.

It has to be mentioned that for reasons of clarity, the control systems are analysed only by their attenuation (Control On minus Control Off). This is why in all of the figures a reduction of the analysed signal caused by the control system is shown by a negative value, while a control-sytem-caused amplification of the signal is shown by a positive value.

Referring to Figure 9, it can easily be seen that the closely collocated control system achieves a higher vibration attenuation at the accelerometer positions. This effect has already been described by Minkoff [21]. It is caused by the over-determined optimisation problem that needs to be solved for the control system with 17 sensors, which explains the lower vibration attenuation at the accelerometers.

Considering that local vibration reductions are not directly correlated to the sound power reduction [18], global measurements like surface velocities and radiated sound power have to be analysed. All informations regarding the global attenuations (Control On minus Control Off) of the 10-sensor and 10-actuator system (10x10 system) has been summarised in Figure 10, the information for the 17-sensor 10-actuator system (17x10 system) in Figure 11.

If we compare first of all the measured sound power reductions, it can be said that the 17x10 system generally achieves a better sound power reduction than the 10x10 system. This effect is noticeable even in the calculated sound power reductions.

For a better visualisation, the amplitudes of the vibration patterns of the uncontrolled centre section, the controlled centre section with the 10x10 system, and the controlled centre section with the 17x10 system are presented in Figures 12, 13, and 14. First of all, it can be observed that the vibration reduction of the closely collocated system occurs only locally, whereas the control system with 17 error sensors generates a more homogeneous vibration reduction.

Referring to the frequency of 268.5 Hz, a global vibration reduction of approximately 6 dB can be achieved for the 17x10 system, which leads to a measured sound power reduction of 6 dB and a calculated sound power reduction of 11 dB. During the sound power measurements, the reproducibility of the measurements was checked and verified. If one assumes that a damping of the vibration pattern occurs only where the shape of the pattern is equal for Control On and Off then the measured sound power reduction appears accurate.

In order to understand difference between the measured and calculated sound power, the outer sections that are not equipped with sensors and actuators are studied. This is why the surface velocities of the left and right section have also been post-processed with the RRM. Afterwards, the sound power of these two sections is averaged and subtracted from the sound power of the active centre section. This difference can be seen as an SNR where a positive value means that the outer sections have lower radiated sound power than the centre section, and a negative value

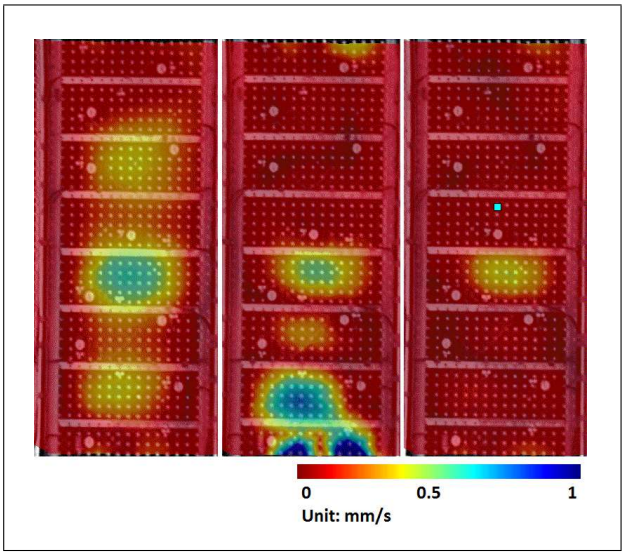

Figure 12. Vibration patterns at 268.5 Hz of the uncontrolled system (left), the controlled system with 10 sensors (centre), and the controlled system with 17 sensors (right).

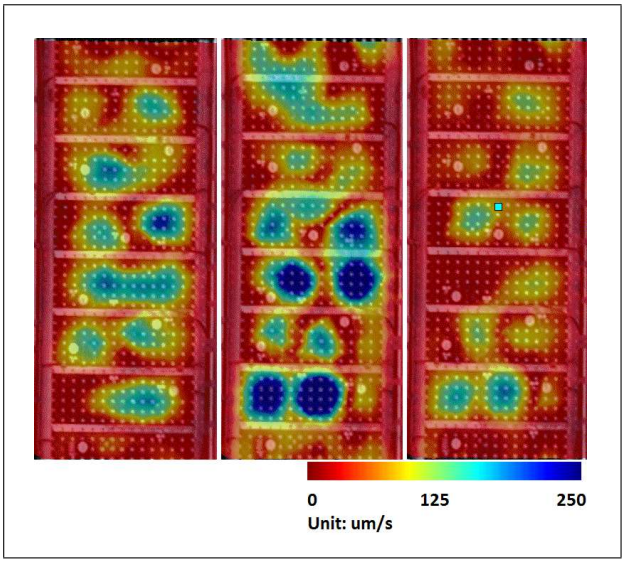

Figure 13. Vibration patterns at 537.2 Hz of the uncontrolled system (left), the controlled system with 10 sensors (centre), and the controlled system with 17 sensors (right).

means that the outer section radiates more sound power than the centre section. The SNR is presented in Figure 15 for all CROR frequencies.

The fact that the SNR is negative in most cases means that the sound power measurement can be disturbed by the outer sections. Especially at 268.5 Hz, the SNR changes from a positive value to a negative value when the controller is switched on. This is due to the high sound power reduction of the centre section and the unaffected sound power of the outer sections. It can thus be stated that the calculated sound power reductions reflect the performance of the active feedforward control system much better than the measured sound power reductions. In previous studies, the accuracy of the sound power calculated by measured velocities and the RRM has been validated by the authors for a slightly curved panel. Then again, the influence of

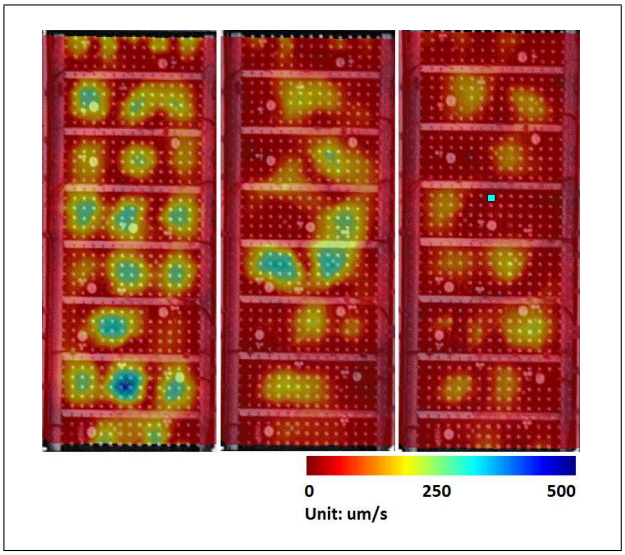

Figure 14. Vibration patterns at 626.9 Hz of the uncontrolled system (left), the controlled system with 10 sensors (centre), and the controlled system with 17 sensors (right).

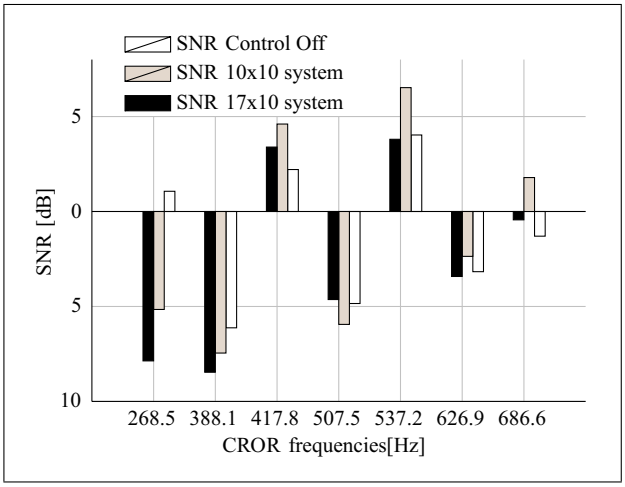

Figure 15. SNR of the measurements.

the vibration of the vertical inner stiffeners on the sound power measurement cannot be excluded.

To further investigate the effects that lead to a sound power reduction or amplification, the radiation efficiency of the vibration patterns is analysed as described in equation (16). The radiation efficiency of the controlled systems decreases in both cases by approximately 10 dB for 268.5 Hz. This reduced radiation efficiency can only be explained by a changed vibration pattern. This effect is visualised in Figure 16 which presents the phase distribution of the 268.5 Hz vibration pattern. It can be seen clearly that in the uncontrolled case, nearly the whole centre section vibrates in phase, whereas the controlled vibration pattern has parts that vibrate in phase and parts that vibrate in antiphase. This alternating regions support the acoustic short-circuit effect.

An example in which the radiation efficiency remains nearly unchanged is the frequency of 537.2 Hz.

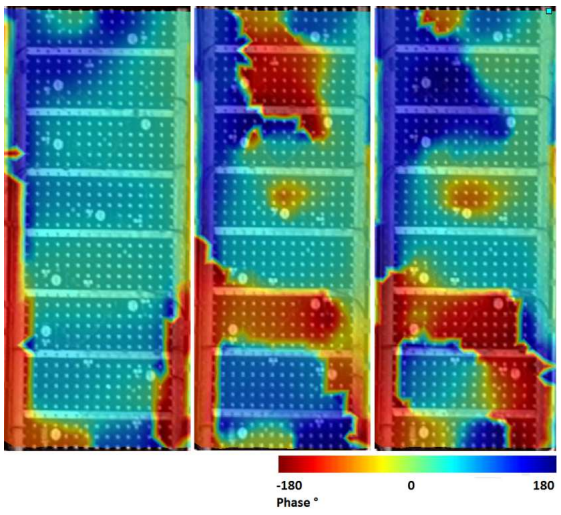

Figure 16. Phase distribution of the centre section at 268.5 Hz of the uncontrolled system (left), controlled system with 10 sensors (centre) and controlled system with 17 sensors (right).

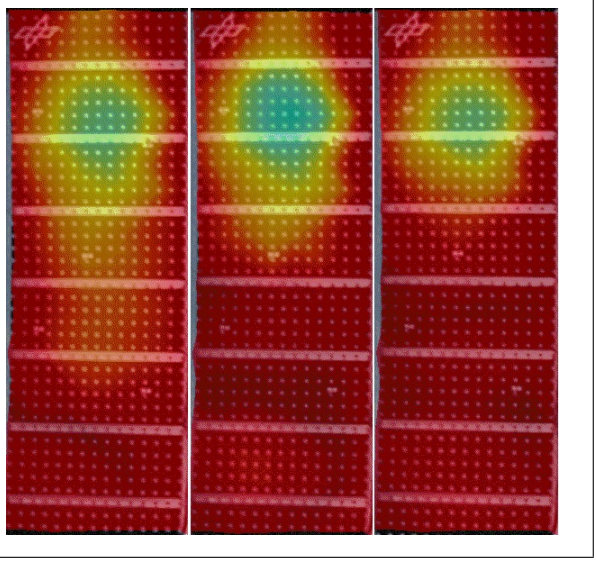

Figure 17. Vibration patterns of the left outer section at 268.5 Hz of the uncontrolled system (left), the controlled system with 10 sensors (centre), and the controlled system with 17 sensors (right).

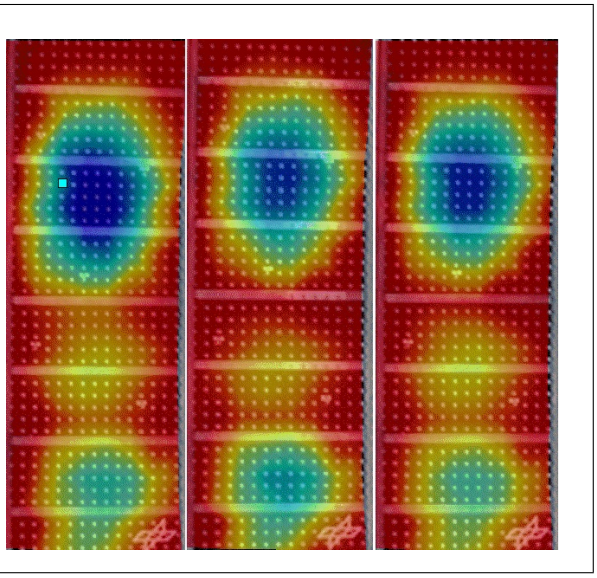

Figure 18. Vibration patterns of the right outer section at 268.5 Hz of the uncontrolled system (left), the controlled system with 10 sensors (centre), and the controlled system with 17 sensors (right).

While this does not mean that the vibration pattern is not restructured, it means that the parts with phase and anti-phase do not change significantly. They are mainly distributed differently, but the ratio of phase and anti-phase regions remains the same. In this case, a global vibration change is directly correlated to a sound power change as seen in Figures 10 and 11.

An increased radiation efficiency can be seen at the frequency of 626.9 Hz. Although both control systems achieve a global vibration attenuation, almost no sound power reduction can be measured or calculated. This is due to a restructured vibration pattern, which radiates sound more efficiently even in the case of lower global amplitudes.

During this investigation another observation has been made. For the first CROR frequencies, where the structural wavelength is relatively large, the outer sections are nearly unaffected by the control system of the centre section. An example is given in Figures 17 and 18 for 268.5 Hz. This effect could be very useful for the application of more decentralised active systems, for example if the active control area has to be expanded over more than two stiffeners. It causes the cross-coupling to be low and means that the interference between the control systems is neglectable. This effect has to be studied further.

6. Conclusion

This paper examines an active feedforward vibration control system for a CFRP fuselage panel excited by a synthesised CROR pressure. Two different control systems were studied: one with 10 closely collocated sensors and actuators and one with 17 sensors and 10 actuators.

In the experiments, a local vibration reduction of 17 dB could be achieved for the closely collocated system and a 6 dB local vibration reduction for the 17x10 system. Furthermore, the measurement data of the global vibration reduction obtained from the LSV revealed a maximum reduction of 6 dB achieved by the 17x10 system at 268.5 Hz. The fact that the 17x10 system leads to a more homogeneous reduction than the 10x10 system is due to its higher observability.

The highest sound power reduction of 11 dB was achieved by the 17x10 system at 268.5 Hz. Furthermore, it can be stated that the global vibration of the fuselage panel was reduced by the 17x10 system for all CROR frequencies except for the 417.8 Hz one. Future work has to

find a way in which the measured sound power of the active section is not disturbed by the inactive outer sections so that the calculated sound power equals the measured one.

A second effect that influences the sound power radiation is the restructuring of the vibration patterns due to the control systems. The radiation efficiency is a measure of how well a vibration pattern is able to radiate sound. In the presented studies, a reduced, an amplified, and an unchanged radiation efficiency can be observed, resulting in a more or less extensive sound power reduction. Several studies show these restructuring problems for feedforward control systems, see for example [25] and [26]. They are mainly caused by new eigenfrequencies and eigenvectors of the controlled structure. This effect is the so-called "pinning" discussed by Gardonio *et al.* [27], which can lead to restructuring in an active vibration control system as the one used in this study. "Pinning" describes the influence of a very high local vibration reduction on the radiation vibration pattern and might be an explanation for the increas ed radiation efficiency of the 10x10 system . In the study of Gardonio *et al.* a reduced vibration attenuation can lead to a higher sound power reduction. In future studies, the feedforward controller should be tuned in order to avoid the "pinning" effect.

Also, an optimisation of the error sensors of the feedforward vibration control system with respect to a global vibration reduction, a lowered radiation efficiency, and the "pinning" effect needs to be attempted in further studies. It can be assumed that an active feedforward vibration control system using these optimised sensors would show an even better performance in sound radiation reduction.

References

[1] F. Farassat, S. Padula, M. Dunn: Advanced turboprop noise prediction based on recent theoretical results. Journal of Sound and Vibration **119** (1987) 53–79.

[2] A. Stuermer, J. Yin: Low-speed aerodynamics and aeroacoustics of cror propulsion systems. Proc. 15th AIAA/ CEAS Aeronautics Conference, 2009.

[3] C. Fuller, C. Rogers, H. Robertshaw: Control of sound radiation with active/adaptive structures. Journal of Sound and Vibration **157** (1992) 19–39.

[4] B. Bingham, M. Atalla, N. Hagood: Comparison of structural-acoustic control designs on an active composite panel. Journal of Sound and Vibration **244** (2001) 761–778.

[5] L. Babu, C. Padmanabhan: Hybrid active and passive noise control of cavities. Acta Acustica united with Acustica **97** (2011) 752–760.

[6] A. Sitel, C. Guigou-Carter, P. Jean: Numerical method for predicting the sound reduction index of a double panel including an active control system and porous material. Acta Acustica united with Acustica **97** (2011) 569–578.

[7] H. Breitbach, D. Sachau, S. Böhme: Acoustic challenges of the a400m for active systems. Smart Structures and Materials, 2006, International Society for Optics and Photonics, 617104ff.

[8] R. Cabell, D. Palumbo, J. Vipperman: A principal component feedforward algorithm for active noise control: Flight test results. IEEE Transactions on Control Systems Technology **9** (2001) 76–83.

[9] B. Petitjean, I. Legrain, F. Simon, S. Pauzin: Active control experiments for acoustic radiation reduction of a sandwich panel: Feedback and feedforward investigations. Journal of Sound and Vibration **252** (2002) 19–36.

[10] E. Bianchi, P. Gardonio, S. Elliott: Smart panel with multiple decentralized units for the control of sound transmission. part iii: Control system implementation. Journal of sound and vibration **274** (2004) 215–232.

[11] M. Misol, S. Algermissen, H. Monner: Experimental investigation of different active noise control concepts applied to a passenger car equipped with an active windshield. Journal of Sound and Vibration (2012).

[12] O. Heintze, M. Misol, S. Algermissen, C. Hartung: Active structural acoustic control for a serial production truck oil pan: Experimental realization. Proceedings of Adaptronic Congress, 2008.

[13] C. R. Fuller, S. Snyder, C. Hansen, R. Silcox: Active control of interior noise in model aircraft fuselages using piezoceramic actuators. AIAA journal **30** (1992) 2613–2617.

[14] D. Palumbo, R. Cabell, J. Cline, B. Sullivan: Flight test of asac aircraft interior noise control system. American Institute of Aeronautics and Astronautics Paper (1999).

[15] P. Gardonio: Review of active techniques for aerospace vibro-acoustic control. Journal of Aircraft **39** (2002) 206–214.

[16] A. Grewal, D. Zimcik, L. Hurtubise, B. Leigh: Active cabin noise and vibration control for turboprop aircraft using multiple piezoelectric actuators. Journal of Intelligent Material Systems and Structures **11** (2000) 438–447.

[17] S. M. Kuo, D. R. Morgan: Active noise control system: Algorithms and dsp implementations. 1.aufl. ed. John Wiley & Sons, Inc., 1996.

[18] S. J. Elliott: Signal processing for active control. 1.aufl. ed. Academic Press, 2001.

[19] F. Fahy, P. Gardonio: Sound and structural vibration: Radiation, transmission and response. Academic Press, 2007.

[20] S. Algermissen, S. Meyer, C. Appel, H. P. Monner: Experimental synthesis of sound pressure fields for active structural acoustic control testing. Proc. 23rd International Conference on Adaptive Structures and Technologies (ICAST), Nanjing (China), 2012.

[21] J. Minkoff: The operation of multichannel feedforward adaptive systems. IEEE Transactions on Signal Processing **45** (1997) 2993–3005.

[22] C. Maury, S. J. Elliott, P. Gardonio: Turbulent boundary-layer simulation with an array of loudspeakers. AIAA journal **42** (2004) 706–713.

[23] C. Maury, T. Bravo: The experimental synthesis of random pressure fields: Practical feasibility. The Journal of the Acoustical Society of America **120** (2006) 2712.

[24] T. Katayama: Subspace methods for system identification. Springer, 2005.

[25] R. Burdisso, C. Fuller: Dynamic behavior of structural-acoustic systems in feedforward control of sound radiation. The Journal of the Acoustical Society of America **92** (1992) 277.

[26] R. Burdisso, C. Fuller: Theory of feedforward controlled system eigenproperties. Journal of Sound and Vibration **153** (1992) 437–451.

[27] P. Gardonio, E. Bianchi, S. J. Elliott: Smart panel with multiple decentralized units for the control of sound transmission. part i: Theoretical predictions. Journal of Sound and Vibration **274** (2004) 163–192.